Available online at www.sciencedirect.com
SCIENCE DIRECT
Journal of Inorganic Biochemistry 100 (2006) 1495–1500
JOURNAL OF Inorganic Biochemistry
www.elsevier.com/locate/jinorgbio

Crystal structure of ferric-yersiniabactin, a virulence factor of *Yersinia pestis*

M. Clarke Miller [a], Sean Parkin [a], Jacqueline D. Fetherston [b], Robert D. Perry [b], Edward DeMoll [a,b,*]

[a] *Department of Chemistry, University of Kentucky Lexington, Chemistry-Physics Building, Room 104, Lexington, Kentucky 40506-0055, United States*
[b] *Department of Microbiology, Immunology and Molecular Genetics, University of Kentucky Lexington, Kentucky 40506, United States*

Received 20 December 2005; received in revised form 6 April 2006; accepted 14 April 2006
Available online 3 May 2006

Abstract

Yersiniabactin (Ybt), the siderophore produced by *Yersinia pestis*, has been crystallized successfully in the ferric complex form and the crystal structure has been determined. The crystals are orthorhombic with a space group of $P2_12_12_1$ and four distinct molecules per unit cell with cell dimensions of $a = 11.3271(\pm0.0003)$ Å, $b = 22.3556(\pm0.0006)$ Å, and $c = 39.8991(\pm0.0011)$ Å. The crystal structure of ferric Ybt shows that the ferric ion is coordinated as a 1:1 complex by three nitrogen electron pairs and three negatively charged oxygen atoms with a distorted octahedral coordination. The molecule displays a Δ absolute configuration with chiral centers at N2, C9, C10, C12, C13, and C19 in R, R, R, R, S, S configurations, respectively. Few of the crystal structures of siderophores have been solved, and those which have been are of simple hydroxamate and catechol types such as ferrioxamine B and agrobactin. To our knowledge this is the first report of the ferric crystal structure of 5-member heterocycle siderophore.

Keywords: Siderophore; *Yersinia pestis*; Yersiniabactin; Crystal; X-ray diffraction

1. Introduction

Iron is an essential element for nearly all forms of life. Although abundant, iron is difficult to obtain from the environment due to its sparing solubility in aqueous solutions under aerobic conditions at neutral pH ($K_{sp} = 10^{-38}$ M^4 for $Fe(OH)_3$, which leads to a soluble hexaaquo ion concentration, $[Fe(OH_2)_6^{3+}] = 10^{-18}$ M at pH 7.0 [1,2]). This problem of iron acquisition also occurs when a pathogenic bacterium invades a host organism where free iron and heme are sequestered by proteins such as transferrin, lactoferrin, hemopexin, hemoglobin, and others. Due to the importance of iron for a myriad of metabolic processes, denial of iron to invading organisms has long been recognized as one of the innate defenses against infection. In fact if iron is withheld from pathogenic bacteria either through genetic or other means, the bacteria do not cause disease [3,4].

In order to overcome these obstacles and survive in a host, pathogenic bacteria have developed elaborate methods to obtain iron that can be generally separated into four mechanisms. Under anaerobic or reducing conditions, ferrous transport systems allow utilization of this more soluble form of iron. Bacterial heme and hemophore transport systems allow the use free as well as protein-complex heme. Some ABC transporters work with microbial receptors for transferrin and lactoferrin for removal and transport of inorganic iron while others do not rely on these receptors for acquisition of inorganic iron. Finally, there is the production of siderophores that chelate precipitated iron from the environment or take it directly host iron-binding proteins. Siderophores are relatively small

* Corresponding author. Address: Department of Chemistry, University of Kentucky Lexington, Chemistry-Physics Building, Room 104, Lexington, Kentucky 40506-0055, United States. Tel.: +1 859 257 7760; fax: +1 859 323 1069.
E-mail address: eldemol@uky.edu (E. DeMoll).

0162-0134/$ - see front matter © 2006 Published by Elsevier Inc.
doi:10.1016/j.jinorgbio.2006.04.007

molecules with extraordinarily high affinities for binding ferric iron. Three categories of siderophore are defined with hydroxamates, catechols, hydroxyacids, or five-member heterocycles as iron coordinating functional groups. Yersiniabactin, along with pyochelin, from *Pseudomonas aeruginosa*, and anguibactin, from *Vibrio anguilarium*, are in this latter group. To be useful a siderophore must have two traits. Firstly, it must be relatively water-soluble since the goal is to manipulate nearly water insoluble iron. Secondly, it must have a higher binding affinity for iron than the biomolecules used by the host to handle and store iron. For example, the transferrin family of glycoproteins share similar iron binding motifs and therefore all have about the same binding constant for iron, $K_D = 10^{-20}$ M. Obviously to compete successfully for iron with biomolecules such as transferrin and lactoferrin, siderophores must have a higher binding affinity. In fact the binding constants for the known siderophore family range from $K_D = 10^{-20}$ M to 10^{-50} M. Enterobactin, which is the siderophore produced by *Escherichia coli*, is reported to have a $K_D = 10^{-52}$ M. That affinity is more than enough to extract iron from transferrin [3–9].

Yersinia pestis, a Gram-negative bacterium, is the causative agent of bubonic plague or Black Death, which devastated Europe in the 14th century. Large reservoirs of this zoonotic disease exist on all inhabited continents except Australia, and the World Health Organization has reported ~2000 human cases of plague each year since the 1950s [10]. Additionally, *Y. pestis* is now considered a potential bioterrorism agent and is classified as a category A select agent [11]. The genome of *Y. pestis* encodes 9 proven or potential inorganic iron transport systems, one heme transport system, and an apparently defective hemophore system [12,13]. Two of these iron transport systems have proven roles in virulence in a mouse model of bubonic plague. The Yfe ABC transporter appears to play a role in the later stages of plague, while the siderophore-dependent yersiniabactin (Ybt) system is essential in the early stages of bubonic plague. Mutants unable to produce or transport the Ybt siderophore are completely avirulent in a mouse model of bubonic plague [14–16]. Indeed, the Ybt siderophore-dependent iron transport system is encoded on pathogenicity islands that are present in the highly virulent strains of *Y. pestis*, *Y. pseudotuberculosis*, and *Y. enterocolitica* as well as a number of enteric pathogens other than *Y. pseudotuberculosis* and *Y. enterocolitica* [17] (see Fig. 1).

In this study, we have examined the structure of the Ybt siderophore, which is made up of one salicylate, one malonate, and three cyclized cysteine residues [18–20]. The mixed non-ribosomal peptide synthetase (NRPS)/polyketide synthetase system which produces Ybt is made up of at least four main enzyme subunits comprising two high molecular weight proteins (HMWP2 and HMWP1), YbtE, and YbtU. It is not known whether these proteins exist in a complex. Synthesis of Ybt begins with YbtE which adenylates a salicylate molecule and loads it onto HMWP2 where two cysteine molecules are then added and cyclized. The

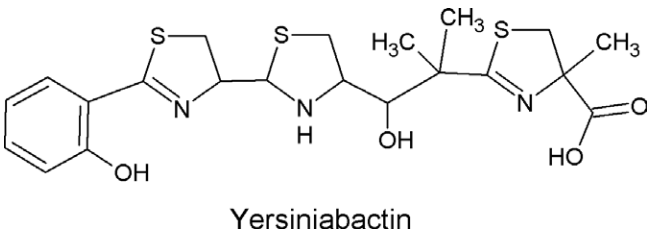

Yersiniabactin

Fig. 1. Structure of yersiniabactin.

substrate is then transferred to HMWP1 where addition, methylation, and reduction of the malonate residue are accomplished. Those steps are followed by the addition and cyclization of the last cysteine residue. At some point YbtU reduces the second thiazoline ring to thiazolidine to produce a mature Ybt molecule. YbtT, a putative thioesterase, likely serves an editing function, removing mischarged or aberrant structures from the enzyme complex [9,13,18–20].

2. Experimental

2.1. Ybt purification

The supernatant was prepared by growing *Y. pestis* KIM6+ in PMH2 media to an A_{620} of 0.80–1.0. The *Y. pestis* KIM6+ strain used for Ybt purification is avirulent due to the lack of an ~70 kb plasmid, pCD1, encoding a type III secretion system and virulence effector proteins. The chemically defined PMH2 medium [21] was rendered iron deficient by extraction with Chelex 100 (BioRad) as previously described [22]. Cells were acclimated to iron-deficient conditions by growth at 37 °C for ~6–8 h and culture supernatants containing Ybt were harvested after growth overnight. Ybt was extracted and purified from the cell supernatant using a four-step modification of a procedure previously described [20]. Supernatants and extracts were protected from light as much as possible while being handled. Approximately 1.5 L of the supernatant was extracted with three 500 ml washes of ethylacetate. The ethylacetate layers were collected, combined, and the solvent was removed by rotary evaporation at 40 °C. The resulting solid material was dissolved in three 5 ml washes of 100% ethanol. The ethanol washes were combined, diluted to 50 ml with water (distilled and de-ionized to 18 MΩ) to 30% ethanol, and then filtered through a 0.22 μm filter. The filter was washed with a minimum (1–2 ml) of ethanol.

The filtrate was then further purified by use of Sep-Pak C-18 mini preparative cartridges. (Waters) Two cartridges were prepared by wetting with 5 ml methanol followed by a 5 ml water wash. The filtrate was loaded onto the cartridges in 25 ml aliquots per cartridge. Each cartridge was then washed with 5 ml of water and eluted with two 5 ml aliquots of methanol. Loading, washing, and elution of the C-18 cartridges were accomplished by gravity feed using a syringe body as a reservoir. The resulting methanol

solution containing Ybt plus various impurities was reduced to 1 ml total volume with a Centrivap concentrator.

Ybt was then isolated using a Waters 600 HPLC equipped with a Waters 996 photodiode array UV/Vis detector and a μRPC C2/C18 ST 4.6/100 column (Amersham Biosciences). Initial injection conditions were 100% water (10 mM ammonium formate pH 8.0 for all solvents except 100% acetonitrile.) immediately followed upon injection by 10 min with 10% acetonitrile/water solution, 160 min of linear gradient to 25% acetonitrile/water solution, ending with 5 min at 100% acetonitrile and a return to 100% water to clean and prepare the column for the next run. The flow rate was 0.5 ml/min. Spectrophotometric data were collected from 200 to 500 nm. The baseline was monitored at 210 nm. Ferric-Ybt and deferrated Ybt eluted at approximately 136 and 144 min, respectively. The identity of the molecule was confirmed by directly extracting the UV–visible spectrum from the data provided by the Waters 996 detector using Waters Empower Pro software. Fractions were collected at 1 min intervals in autoclaved 1.5 ml micro-centrifuge tubes and stored frozen at −20 ° C for later use.

Finally, the collected ferric-Ybt containing fractions were combined and loaded onto a C-18 reverse phase cartridge, eluted, and methanol was removed by evaporation. In this case the material was taken to dryness in a Centrivap concentrator. The resulting dark yellow to light brown material was then subjected to crystallization procedures.

2.2. Ybt crystallization

Several crystallization methods were attempted. However, the method that finally yielded useful crystals is described herein. Approximately 10 mg of the purified ferric Ybt was dissolved in a minimal amount (roughly 300–500 μl) of diethyl ether, placed in a 1 ml glass vial and then carefully layered with an equal volume of hexane. The mixture was protected from light and allowed to remain undisturbed at room temperature for several days. In about five days small, copper colored, needle shaped crystals were observed in the flask. After 2–3 more days the crystals reached their maximum size of about 1.0 to 1.5 mm × 0.05 mm (see Fig. 2).

2.3. Crystal structure determination

The thin needle-shaped crystals obtained proved too small for conventional small-molecule diffraction equipment but diffracted well at 90K (CryoIndustries of America CryoCool LN_2) on a hybrid small/macromolecule machine based on the Bruker X8 Proteum (SMART 6000 detector, Nonius Kappa goniometer). Data were collected using Cu Kα radiation (Nonius FR591 rotating anode generator, Montel graded multilayer optics). Initial unit cell parameters were obtained using APEX2 software [23] from diffraction spot positions in six 10° ω-scans at different φ and χ angles. Final cell parameters were refined in a least-squares scheme (program SaintPlus in APEX2) using spot positions from all data collection frames. Crystal

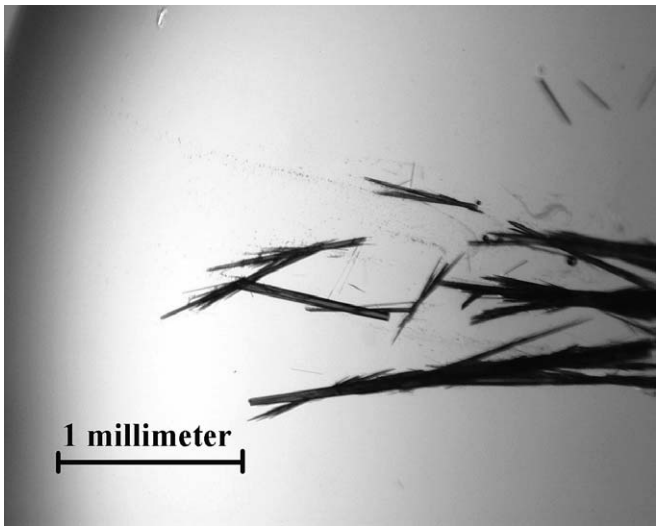

Fig. 2. Yersiniabactin-Fe^{III} crystals. The color is deep red. The roughly 1 millimeter crystal just below center, aligned at an approximately 160° angle, was chosen for X-ray analysis. The crystal was broken roughly in half and the right hand side, as pictured, was utilized.

Table 1
Crystal data and experimental parameters

Empirical formula	$C_{21}H_{23}FeN_3O_4S_3$
Formula weight	533.45 g/mol
Temperature	90.0(2) k
Wavelength	1.54178 Å
Crystal system	Orthorhombic
Space group	$P2_12_12_1$
Unit cell dimensions	$a = 11.3271(3)$ Å
	$b = 22.3556(6)$ Å
	$c = 39.8991(11)$ Å
	$\alpha = 90°$
	$\beta = 90°$
	$\gamma = 90°$
Volume	10103.4(5) $Å^3$
Z	16
D_{calc}	1.403 Mg/m^3
Absorption coefficient	7.371 mm^{-1}
$F(000)$	4768
Crystal size	0.35 × 0.04 × 0.03 mm
θ range	2.21–68.09°
Limiting indices	$-3 \leqslant h \leqslant 12$
	$-26 \leqslant k \leqslant 26$
	$-46 \leqslant l \leqslant 47$
Reflections collected/unique	64,190/17493 [$R_{int} = 0.0738$]
Completeness to $\theta = 68.09$	96.7%
Maximum and minimum transmission	0.8027 and 0.6613
Refinement method	Full-matrix least-squares on F^2
Data/restraints/parameters	17,493/1299/1249
Goodness-of-fit on F^2	1.018
Final R indices [$I > 2\sigma(I)$]	$R_1 = 0.0556$, $wR_2 = 0.1138$
R indices (all data)	$R_1 = 0.0821$, $wR_2 = 0.1262$
Absolute structure parameter	−0.001(4)
Extinction coefficient	0.000035(8)
Largest ΔF peak and hole	0.587 and −0.597 e/$Å^3$

Table 2
Bond lengths or angles (Å or degrees [°]) for each molecule of the unit cell of the Ybt-Fe^{+3} crystal

	A	B	C	D
Fe(1)–O(2)	1.899(4)	1.886(4)	1.904(4)	1.906(4)
Fe(1)–O(1)	1.920(4)	1.924(4)	1.928(4)	1.925(4)
Fe(1)–O(3)	2.078(4)	2.074(5)	2.085(4)	2.099(4)
Fe(1)–N(1)	2.084(5)	2.069(4)	2.055(5)	2.038(5)
Fe(1)–N(3)	2.130(5)	2.133(5)	2.131(5)	2.106(5)
Fe(1)–N(2)	2.255(5)	2.244(5)	2.218(5)	2.213(4)
N(1)–C(7)	1.262(7)	1.286(7)	1.284(7)	1.296(7)
N(1)–C(9)	1.470(7)	1.473(7)	1.455(8)	1.459(8)
N(2)–C(10)	1.477(7)	1.483(7)	1.468(7)	1.461(7)
N(2)–C(12)	1.495(7)	1.506(7)	1.486(7)	1.484(7)
N(3)–C(17)	1.285(7)	1.289(8)	1.277(7)	1.279(7)
N(3)–C(19)	1.466(7)	1.477(7)	1.467(7)	1.471(7)
O(1)–C(1)	1.313(7)	1.333(7)	1.323(7)	1.324(7)
O(2)–C(13)	1.392(7)	1.377(8)	1.396(7)	1.402(6)
O(3)–C(21)	1.276(7)	1.280(7)	1.281(7)	1.278(7)
O(4)–C(21)	1.225(6)	1.222(6)	1.247(7)	1.231(7)
S(1)–C(7)	1.788(7)	1.775(6)	1.749(7)	1.755(6)
S(1)–C(8)	1.812(8)	1.809(7)	1.807(7)	1.819(7)
S(2)–C(10)	1.809(6)	1.812(7)	1.810(6)	1.812(6)
S(2)–C(11)	1.816(6)	1.815(6)	1.832(6)	1.823(6)
S(3)–C(17)	1.742(6)	1.737(7)	1.754(6)	1.738(6)
S(3)–C(18)	1.821(6)	1.815(6)	1.826(6)	1.813(6)
C(8)–C(9)	1.529(8)	1.513(8)	1.541(8)	1.541(8)
C(11)–C(12)	1.529(9)	1.533(9)	1.540(8)	1.516(8)
C(18)–C(19)	1.524(8)	1.526(9)	1.539(8)	1.547(8)
O(2)–Fe(1)–O(1)	102.56(18)	101.64(18)	105.42(17)	104.27(17)
O(2)–Fe(1)–O(3)	159.61(17)	160.68(18)	158.14(17)	155.67(16)
O(1)–Fe(1)–O(3)	93.34(17)	94.74(17)	93.22(16)	97.33(17)
O(2)–Fe(1)–N(1)	99.87(18)	95.79(19)	97.17(18)	99.84(19)
O(1)–Fe(1)–N(1)	86.20(18)	85.95(18)	84.88(18)	85.52(18)
O(3)–Fe(1)–N(1)	93.78(16)	95.50(16)	95.75(17)	92.81(18)
O(2)–Fe(1)–N(3)	87.08(17)	88.36(18)	86.94(18)	88.49(18)
O(1)–Fe(1)–N(3)	108.85(18)	111.41(19)	109.94(18)	103.42(18)
O(3)–Fe(1)–N(3)	75.64(16)	76.07(17)	75.84(16)	75.56(17)
N(1)–Fe(1)–N(3)	161.80(18)	161.01(19)	163.07(18)	166.01(19)
O(2)–Fe(1)–N(2)	78.64(17)	77.82(18)	78.95(17)	79.19(16)
O(1)–Fe(1)–N(2)	163.79(18)	163.42(18)	162.61(18)	163.48(18)
O(3)–Fe(1)–N(2)	89.66(16)	89.38(17)	86.65(16)	83.29(17)
N(1)–Fe(1)–N(2)	77.71(18)	77.67(18)	77.84(19)	77.96(18)
N(3)–Fe(1)–N(2)	87.32(18)	85.16(19)	86.92(18)	92.76(18)
C(7)–N(1)–C(9)	115.4(5)	114.0(5)	115.7(5)	115.8(5)
C(7)–N(1)–Fe(1)	128.1(4)	129.1(4)	127.7(5)	127.5(4)
C(9)–N(1)–Fe(1)	115.7(4)	114.7(3)	116.0(4)	116.3(4)
C(7)–S(1)–C(8)	89.8(3)	89.2(3)	91.9(3)	91.5(3)
N(1)–C(7)–S(1)	113.8(5)	114.0(5)	115.7(5)	115.5(5)
C(9)–C(8)–S(1)	103.8(4)	104.0(4)	106.5(4)	106.8(4)
N(1)–C(9)–C(8)	106.7(5)	106.4(5)	110.0(5)	109.5(5)
C(10)–N(2)–C(12)	111.8(5)	110.5(5)	112.6(5)	111.8(4)
C(10)–N(2)–Fe(1)	112.9(3)	111.4(4)	110.6(4)	111.9(3)
C(12)–N(2)–Fe(1)	108.2(3)	108.1(4)	108.1(3)	107.8(3)
C(10)–S(2)–C(11)	88.3(3)	89.1(3)	88.1(3)	87.2(3)
N(2)–C(10)–S(2)	107.3(4)	107.8(4)	105.6(4)	107.3(4)
C(12)–C(11)–S(2)	105.5(4)	106.6(4)	105.6(4)	105.3(4)
N(2)–C(12)–C(11)	108.2(5)	109.7(5)	108.1(5)	108.3(5)
C(17)–N(3)–C(19)	115.0(5)	113.5(5)	115.7(5)	115.4(5)
C(17)–N(3)–Fe(1)	126.6(4)	126.1(4)	127.3(4)	124.2(4)
C(19)–N(3)–Fe(1)	115.2(3)	115.6(3)	114.4(4)	114.0(4)
C(17)–S(3)–C(18)	90.9(3)	90.0(3)	90.4(3)	91.1(3)
N(3)–C(17)–S(3)	115.6(4)	116.5(5)	115.7(4)	117.2(4)
C(19)–C(18)–S(3)	105.6(4)	105.2(4)	105.7(4)	107.5(4)
N(3)–C(19)–C(18)	108.7(5)	107.9(5)	108.2(5)	108.7(5)

decay (negligible) was checked by re-measurement of a portion of the first data collection scan. A total of 64,190 reflections were collected that gave 17,493 unique reflections after merging of symmetry equivalents, 13,923 of which had intensity $I > 2\sigma(I)$. Correction of Lorentz and polarization effects, data reduction, merging and an empirical absorption correction were performed within the APEX2 package (programs SaintPlus and Sadabs). The structure was solved by direct methods using SHELXS97 and refined by full-matrix least-squares against F^2 using SHELXL97 [24]. All non-hydrogen atoms of the four crystallographically independent main molecules and one ether (occluded solvent) molecule were refined with anisotropic displacement parameters subject to a rigid-body restraint (command 'DELU' in SHELXL97). A second, rather ill-defined ether molecule, was refined as disordered over two overlapping positions (in the ratio 61–39%) with isotropic displacement parameters and similarity restraints (command 'SAME' in SHELXL97). The absolute configuration was determined by refinement of Flack's parameter, $x(u) = -0.001(4)$ [25]. Hydrogens attached to all ordered atoms were found in difference Fourier maps and were subsequently placed (along with hydrogens attached to disordered groups) at calculated positions using appropriate riding models with C–H distances of 0.95 Å (C_{ar}–H), 0.98 Å (C–H_3), 0.99 Å (C–H_2), 1.00 Å (C–H). Isotropic displacement parameters were fixed at either 1.2 times (C_{ar}–H, C–H, C–H_2) or 1.5 times (C–H3) the U_{eq} of the carrier atom. Data collection details, crystal data, and refinement parameters are summarized in Table 1. Selected bond lengths and angles are given in Table 2.

3. Results and discussion

Siderophores are of interest for study for several reasons. Members of the family of the genus *Pseudomonas*, which occur in soil and promote plant growth, are thought to do so in part by utilizing siderophores to deprive endemic root colonizing phytopathogenic microorganisms of ferric iron. Understanding this process could lead to improved agricultural methods of promoting plant growth and controlling phytopathogens without the need for potentially environmentally harmful chemicals [26]. Examples of medical applications of siderophores include the use of Desferral which is the mesylate salt of deferrioxamine B, a siderophore produced by *Streptomyces pilosus*, for treatment of iron toxicity [27]. The potency of many common antibiotics has been increased by including elements from siderophores into their structure [28]. Because of their virulence role in a number of pathogens and similarities between some siderophores (e.g. Ybt and pyochelin), siderophore-dependent iron transport systems are an obvious target for development of new antimicrobial therapies as resistances to traditional antibiotics continue to develop [29]. It is interesting that in light of the importance of siderophores surprisingly few of the crystal structures of siderophores have been solved, and those are of simple

hydroxamate and catechol types [30–33]. To our knowledge this is the first report of the ferric crystal structure of a 5-member heterocycle siderophore (see Figs. 3 and 4).

From the initial observations of the Ybt structure [18–20] a question arose as to why only the middle of the three cyclocysteine rings has a reduced double bond. Several hypotheses were proposed to explain the need for this modification. The reduction may be required for the completion of the synthesis of the rest of the Ybt molecule or for the subsequent release of the final product as with pyochelin, a similar siderophore produced by *Pseudomonas aeruginosa*. In the case of pyochelin the second thiazoline ring must be reduced to thiazolidine for nucleophilic interaction with a methyl transferase domain. The modification could also be required to maintain the stability of the siderophore by preventing relatively facile oxidation of the thiazoline ring to a heteroaromatic thiazole. Another possibility is that the reduction, or lack thereof, of one or both of these cysteine residues could be responsible for gating the enzyme reaction. For example, transfer from HMWP2 to HMWP1 or activity of YbtT, the final thioesterase responsible for release of the finished siderophore, may be mediated by the oxidation state of the thiazoline rings [34–36].

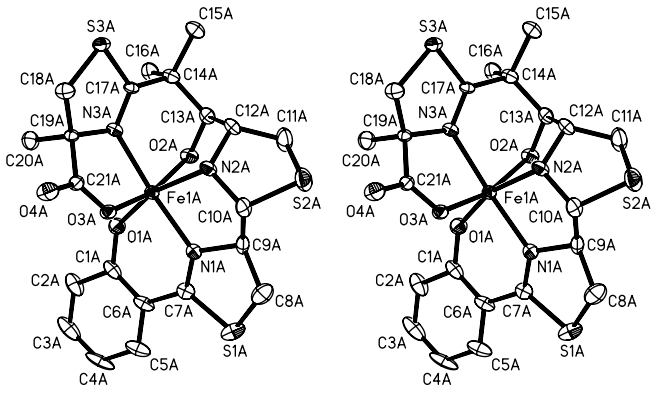

Fig. 3. 50% probability thermal ellipsoid plot with the atomic numbering scheme showing the coordination geometry of yersiniabactin-Fe^{III}. Hydrogen atoms have been omitted for clarity.

An additional, not exclusive, hypothesis is that the reduction allows more flexibility in the Ybt molecule by giving it more degrees of freedom in forming the complex. In ferric-Ybt the iron atom is coordinated by three nitrogen electron pairs and three negatively charged oxygen atoms, a phenolate oxygen, a carboxylate oxygen, and the oxygen from a secondary alcohol. That this last ligand did not retain the proton was surprising, however there was clearly no electron density corresponding to an alcoholic hydrogen atom present in the crystal. These six ligands are arranged in a distorted octahedral arrangement (see Table 2 for bond lengths and angles). The nitrogen of the reduced, cyclized cysteine ring occupies the iron orbital that is encountered after the change of plane of the Ybt molecule during its wrapping around all of the coordination points. The change of plane seemingly requires a greater stretch than in going between orbitals in the same plane, as the length of this bond to iron is the longest, by 0.1 Å of all of the ligands, and longer than reported for bonds in other siderophore structures except for the similar Micacocidin A

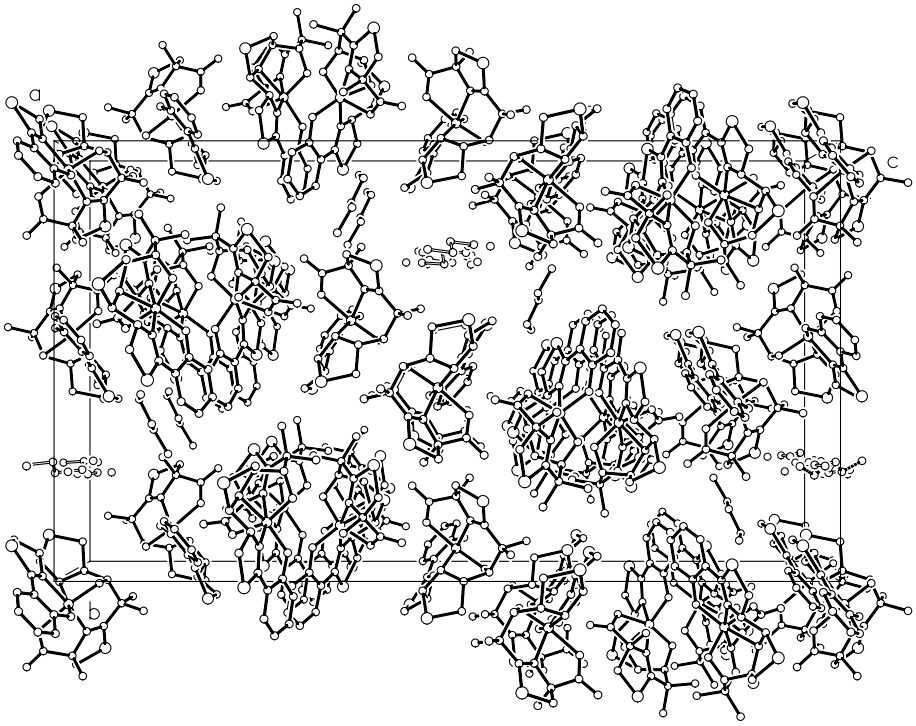

Fig. 4. Representation of the crystal packing plot along the *A* axis. The four distinct molecules making up the unit cell are clearly visible at the center.

antibiotic, where the analogous bond is actually 0.1 Å longer still [30,32].

Micacocidin A, a compound of similar chemical structure to Ybt was crystallized with a Zn^{II} ion coordinated octahedrally by analogous ligands to those in the ferric-Ybt complex. The Zn compound was isolated from the culture filtrate of *Pseudomonas* sp. No. 57–250 [37]. It acts as an antibiotic toward bacteria of the genus *Mycoplasma*. Whether Micacocidin A has a significant affinity for Fe^{III} is not known, however it would be surprising if a compound with such a similar structure to Ybt, as Micacocidin A, would not bind Fe^{III}. However, the fact that molecules as similar as Micacocidin A and Ybt preferentially coordinate different metal ions could also point out that seemingly slight differences in siderophore structure can confer different metal specificities. One significant difference in the Ybt and Micacocidin A structures is that the oxygen of the secondary alcohol apparently retains its hydrogen atom in the Micacocidin A crystal structure, whereas in Ybt-Fe^{III} the hydrogen is lost and the ligand is the negatively charged oxygen atom. Perhaps it is necessary for the net charge on the complex to be zero. This is the case for both the Zn^{II}-Micacocidin A complex and the Fe^{III}-Ybt complex. This property might also account for the significant lack of affinity of Ybt for binding Fe^{II} [20].

Acknowledgements

This work was supported by Public Health Service grant AI33481 to ED, JDF, and RDP from the National Institutes of Health. We would also like to thank Mr. Jeff Withers for his insight and for technical discussions with him.

Appendix A. Supplementary data

Supplementary data associated with this article can be found, in the online version, at doi:10.1016/j.jinorgbio.2006.04.007.

References

[1] S. Dhungana, A. Crumbliss, Geomicrobiol. J. 22 (2005) 87–98.
[2] H. Boukhalfa, A. Crumbliss, BioMetals 15 (2002) 325–339.
[3] B.R. Byers, E.L. Arceneaux, in: A. Sigel, H. Sigel (Eds.), Metal Ions in Biological Systems: Iron Transport and Storage in Microorganisms, Plants, and Animals, vol. 35, Marcell Dekker Inc., New York, 1998, pp. 37–66.
[4] K.N. Raymond, E.A. Dertz, in: J.H. Crosa, A.R. Mey, S.M. Payne (Eds.), Iron Transport in Bacteria, ASM Press, Washington, DC, 2004, pp. 3–17.
[5] V. Braun, K. Hantke, W. Köster, in: A. Sigel, H. Sigel (Eds.), Metal Ions in Biological Systems: Iron Transport and Storage in Microorganisms, Plants, and Animals, vol. 35, Marcel Dekker Inc., New York, 1998, pp. 67–145.
[6] L. Debarieux, C. Wandersman, in: J.H. Crosa, A.R. Mey, S.M. Payne (Eds.), Iron Transport in Bacteria, ASM Press, Washington, DC, 2004, pp. 38–47.
[7] K. Hantke, in: J.H. Crosa, A.R. Mey, S.M. Payne (Eds.), Iron Transport in Bacteria, ASM Press, Washington, DC, 2004, pp. 178–184.
[8] D. Perkins-Balding, A. Rasmussen, I. Stojiljkovic, in: J.H. Crosa, A.R. Mey, S.M. Payne (Eds.), Iron Transport in Bacteria, ASM Press, Washington, DC, 2004, pp. 66–85.
[9] C.T. Walsh, C.G. Marshall, in: J.H. Crosa, A.R. Mey, S.M. Payne (Eds.), Iron Transport in Bacteria, ASM Press, Washington, DC, 2004, pp. 18–37.
[10] R.D. Perry, J.D. Fetherston, Clin. Microbiol. Rev. 10 (1997) 35–66.
[11] T.V. Inglesby et al., J. Am. Med. Assoc. 283 (2000) 2281–2290.
[12] R.D. Perry, in: J.H. Crosa, A.R. Mey, S.M. Payne (Eds.), Iron Transport in Bacteria, ASM Press, Washington, DC, 2004, pp. 219–240.
[13] R.D. Perry, J.D. Fetherston, in: E. Carniel, B.J. Hinnebusch (Eds.), *Yersinia* Molecular and Cellular Biology, Horizon Bioscience, Norfolk, UK, 2004, pp. 257–283.
[14] S.W. Bearden, J.D. Fetherston, R.D. Perry, Infect. Immunity 65 (1997) 1659–1668.
[15] S.W. Bearden, R.D. Perry, Mol. Microbiol. 32 (1999) 403–414.
[16] J.D. Fetherston, V.J. Bertolino, R.D. Perry, Mol. Microbiol. 32 (1999) 289–299.
[17] B. Lesic, E. Carniel, in: E. Carniel, B.J. Hinnebusch (Eds.), *Yersinia* Molecular and Cellular Biology, Horizon Bioscience, Norfolk, UK, 2004, pp. 285–306.
[18] C.E. Chambers, D.D. McIntyre, M. Mouck, P.A. Sokol, BioMetals 9 (1996) 157–167.
[19] H. Drechsel, H. Stephan, R. Lotz, H. Haag, H. Zähner, K. Hantke, G. Jung, Liebigs Ann. (1995) 1727–1733.
[20] R.D. Perry, P.B. Balbo, H.A. Jones, J.D. Fetherston, E. DeMoll, Microbiology 145 (1999) 1181–1190.
[21] S. Gong, S.W. Bearden, V.A. Geoffroy, J.D. Fetherston, R.D. Perry, Infect. Immunity 67 (2001) 2829–2837.
[22] T.M. Staggs, R.D. Perry, J. Bacteriol. 173 (1991) 417–425.
[23] Bruker-Nonius, APEX2: software suite for data collection and processing of single crystal X-ray diffraction data, Madison, WI, USA, 2004.
[24] G.M. Sheldrick, SHELX-97: Programs for the solution (SHELXS97) and refinement (SHELXL97) of crystal structures from diffraction data, 1997.
[25] H.D. Flack, G. Bernardinelli, Acta Cryst. A 55 (1999) 908–915.
[26] J.S. Buyer, J. Leong, J. Biochem. 261 (1986) 791–794.
[27] R.J. Bergeron, G.M. Brittenh (Eds.), The development of Iron Chelators for Clinical Use, CRC Press, Boca Raton, FL, 1994.
[28] N.A. Watanabe, T. Nagasu, K. Katsu, K. Kitoh, Antimicrob. Agents Chemotherp. 31 (1987) 497–504.
[29] M. Galimand et al., New England Journal of Medicine 337 (1997) 677–680.
[30] S. Dhungana, P. White, A. Crumbliss, J. Bio. Inorg. Chem. 6 (2001) 810–818.
[31] M. Teintze, M.B. Hossain, C.L. Barnes, J. Leong, D. van der Helm, Biochemistry 20 (1981) 6446–6457.
[32] M. Teintze, J. Leong, Biochemistry 20 (1981) 6457–6462.
[33] D. van der Helm, M.A.F. Jalal, M.B. Hossain, in: G. Winkelmann, D. van der Helm, J.B. Neilands (Eds.), Iron Transport in Microbes, Plants and Animals, VCH Publishers, New York, NY, 1987, pp. 135–165.
[34] D.A. Miller, L. Luo, N. Hillson, T.A. Keating, C.T. Walsh, Chem. Biol. 9 (2002) 333–344.
[35] L.E.N. Quadri, T.A. Keating, H.M. Patel, C.T. Walsh, Biochemistry 38 (1999) 14941–14954.
[36] C.T. Walsh, H. Chen, T.A. Keating, B.K. Hubbard, H.C. Losey, L. Luo, C.G. Marshall, D.A. Miller, H.M. Patel, Current Opinion in Chemical Biology 5 (2001) 525–534.
[37] H. Nakkai, S. Kobayoshi, M. Ozaki, Y. Hayase, R. Takeda, Acta Cryst. C 55 (1999) 54–56.